

Theory of optically-induced dispersion forces between weakly-disordered Van der Waals crystals

Jonas von Milczewski^{1,2,3} and John R. Tolsma^{3,*}

¹Max-Planck-Institute of Quantum Optics, Hans-Kopfermann-Straße 1, 85748 Garching, Germany

²Munich Center for Quantum Science and Technology, Schellingstraße 4, 80799 Munich, Germany

³Institute for Theoretical Physics, ETH Zurich, 8037 Zurich, Switzerland

(Dated: March 18, 2019)

We describe a many-body theory for interlayer dispersion forces between weakly disordered atomically-thin crystals and numerically investigate the role of disorder for different layer-separation distances and for different densities of optically-induced electrons and holes. In contrast to the common wisdom that disorder tends to enhance the importance of Coulomb interactions in Fermi liquids, we find that short-range disorder tends to *weaken* interlayer dispersion forces. We demonstrate that disorder alters the scaling laws of dispersion forces and we comment on the role of the maximally-crossed vertex-correction diagrams responsible for logarithmic divergences in the resistivity of two-dimensional metals.

PACS numbers: 73.20.-r,71.15.-m,71.10.-w, 73.21.-b,75.10.-b

I. INTRODUCTION

Even when two objects are each electrically neutral, forces between the two objects which are mediated by the electromagnetic field can still be present. These *dispersion* forces were named by F. London in his theoretical investigation of forces between molecules¹. Although each molecule has zero total charge, quantum fluctuations in the charge-density of each molecule leads to an effective dipole-dipole intermolecular force. This mechanism was later generalized by Lifshitz² to describe forces between solids, wherein he discovered a force which scales like $1/d^3$ when the distance between two thick slabs becomes large. Depending on the context, these forces also go under the name of Van der Waals or Casimir forces, where the former (latter) often indicates that the force is mediated by the longitudinal (transverse) component of the electromagnetic gauge field³.

Dispersion forces are relatively weak and short-ranged compared to electrostatic forces, and are difficult to observe in experiments on solids. Recently however, advances in X-ray spectroscopy have allowed for atomic-level precision measurements of interlayer strain in thin-films and atomically-thin crystals^{4,5}, and signatures consistent with interlayer dispersion forces among optically-induced electrons and holes have been measured in transition-metal dichalcogenide multilayers⁶. This adds a new experimentally measurable quantity to the class of phenomena which are sensitive to correlations amongst quasiparticles in neighboring layers of atomically-thin crystals like transition-metal dichalcogenides, graphene, twisted bilayer graphene, and phosphorene. Coulomb drag⁷ is a notable example of the type of phenomena which are sensitive to interlayer correlations,. In these experiments a current is driven in one layer and as a result of interlayer Coulomb interactions an induced voltage drop appears in a second (otherwise passive) nearby layer. Drag experiments have led to a deeper under-

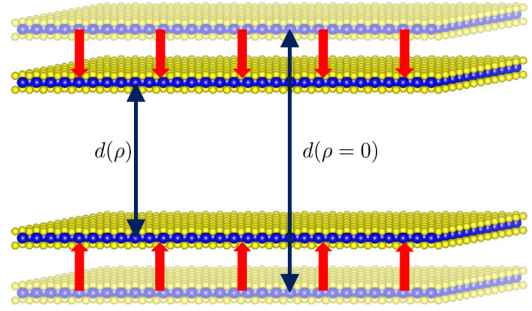


FIG. 1: An illustration of the change in interlayer separation distance, $d(\rho) - d(0)$, which result from the attractive forces between layers that is induced by optically creating a finite density of electrons and holes in each layer, ρ .

standing of the nature of the elementary excitations and ground-state wavefunctions of complex phases of matter, from two-dimensional Fermi liquids to more exotic phases like exciton condensates^{8,9} and Luttinger liquids¹⁰. Just like Coulomb drag, the interlayer dispersion force between atomically thin crystals offers an interesting test-bed for the various many-body theories describing the complex behavior of solids.

In this article we construct many-body approximations to explore the impact of weak disorder on the interlayer dispersion forces which act between layers of a bilayer heterostructure after a finite density of electrons and holes are induced in each layer by an optical pulse. While *ab initio* methods for obtaining Van der Waals contributions to the ground-state energy exist¹¹, our diagrammatic approach is sensitive to the exchange-correlation effects which density-functional theory usually deals with only on a mean-field level using variations of the local-density approximation; the approach discussed in this paper is complimentary to these existing tools and allows for the treatment of systems with strongly corre-

lated ground-states or, as we investigate in detail below, random disorder. Quasiparticle-impurity interactions are known to be responsible for a number of fascinating properties of metals, from weak-localization corrections to the longitudinal conductivity¹² to anomalies in the tunneling conductivity^{13,14}, and we will make use of some of these well-developed many-body approximations in determining the role of weak disorder on interlayer dispersion forces.

Our paper is organized as follows. In section II we describe a many-body theory for the interlayer dispersion force based on a linked-cluster expansion for the correlation energy of a bilayer in the absence of disorder. In the limit of high quasiparticle density and large separation distance, we recover the same scaling behavior as found by Lifshitz for thick slabs separated by a distance d . In section III we describe a leading-order-in- $1/\varepsilon_F\tau$ theory for interlayer forces. We demonstrate that disorder qualitatively alters the scaling laws and demonstrate that, surprisingly, disorder tends to reduce the magnitude of interlayer forces. In section IV we discuss the impact on interlayer forces by a class of Feynman diagrams known to yield logarithmic divergences in the longitudinal resistivity of two-dimensional metals. Finally in section V we summarize our conclusions and discuss interesting questions to address in the future.

II. OPTICALLY-INDUCED DISPERSION FORCES IN BILAYER SYSTEMS

We consider a system governed by the following Hamiltonian

$$\mathcal{H} = \mathcal{H}_0 + \mathcal{H}_{e-e} + \mathcal{H}_{e-imp} \quad (1)$$

which describes the kinetic energy of electrons and holes, the Coulomb interaction, and the interaction of electrons and holes with impurities, respectively. We assume, as is often the case experimentally, that the density of electrons and holes (quasiparticles) induced by the optical excitation is such that the kinetic energy of electrons and holes can be described by an effective mass approximation,

$$\mathcal{H}_0 = \sum_{\mathbf{k}\alpha I} \varepsilon_\alpha(\mathbf{k}) \hat{a}_{\mathbf{k}\alpha I}^\dagger \hat{a}_{\mathbf{k}\alpha I}, \quad (2)$$

where $\varepsilon_\alpha(\mathbf{k}) = \hbar^2 k^2 / 2m_\alpha$ and α is a composite index which labels the spin, valley, and band (e.g. valence *vs.* conduction band) quantum numbers. In the following we will consider the limit in which interlayer hopping is weak compared to the exchange-correlation energy per electron. Thus, the single-particle wavefunctions have a which-layer quantum number, which we label by I . Interlayer hybridization of the conduction and valence bands are notoriously weak in Van der Waals crystals (as the name suggests) and are often further weakened by rotational misalignment of neighboring layers. We comment

below on how our theory can be straight-forwardly generalized to incorporate interlayer hybridization when it becomes important.

The charged quasiparticles in the various layers of the system interact with each other via the Coulomb interaction

$$\mathcal{H}_{e-e} = \frac{1}{2L^2} \sum_{\substack{\mathbf{q} I J \\ \mathbf{k}_1 \mathbf{k}_2 \\ \alpha \beta}} V_{IJ}(\mathbf{q}) \hat{a}_{\mathbf{k}_1+\mathbf{q}\alpha I}^\dagger \hat{a}_{\mathbf{k}_2-\mathbf{q}\beta J}^\dagger \hat{a}_{\mathbf{k}_2\beta J} \hat{a}_{\mathbf{k}_1\alpha I}, \quad (3)$$

where

$$V_{IJ}(\mathbf{q}) = \begin{cases} 2\pi e^2 / (\kappa q) & I = J \\ 2\pi e^2 e^{-q d} / (\kappa q) & I \neq J. \end{cases} \quad (4)$$

The material-specific parameter, κ , describes the dielectric contributions of the elementary excitations outside of our model (e.g. phonons). The strength of Coulomb interactions is traditionally¹⁵ described by the value of a parameter r_s which expresses the ratio of average interaction energy to average kinetic energy in a disorder-free 2DEG, $r_s \propto \langle \mathcal{H}_{e-e} \rangle / \langle \mathcal{H}_0 \rangle$. The parameter depends on the total density of electrons (and holes) in each layer, n_I , and is larger when the density is lower, $r_s = [\pi (a_B^* n_I)^2]^{-1}$. Here, $a_B^* = \kappa a_B / m_{eff}$, is the effective Bohr radius. When the system contains several effective masses it is useful to define a_B^* using the geometric mean of the masses, $m_{eff} \rightarrow (\prod_\alpha m_\alpha)^{\frac{1}{|\alpha|}}$. Interactions of charged quasiparticles in different layers are ultimately responsible for the optically-induced Van der Waals forces we describe. In this article we consider densities of optically-induced quasiparticles which are large enough to form electron-liquids and hole-liquids rather than excitons, as was recently demonstrated at room temperature¹⁶.

The interaction between electrons and holes and the impurities of the crystal is obtained by assuming that each impurity creates a deviation in the perfectly periodic scalar potential created by the underlying lattice. This scalar potential couples linearly to the density of electrons and holes,

$$\mathcal{H}_{e-imp} = \frac{1}{L^2} \sum_{\mathbf{Q}, I} u_I(\mathbf{Q}) \rho_I(\mathbf{Q}) \sum_{\mathbf{k}\alpha} \hat{a}_{\mathbf{k}+\mathbf{Q}\alpha I}^\dagger \hat{a}_{\mathbf{k}\alpha I} \quad (5)$$

where $\rho_I(\mathbf{Q})$ is the Fourier transform of the density of impurities in layer I , and $u_I(\mathbf{Q})$ is the Fourier transform of the scalar potential of each impurity. We assume that electrons only scatter off the impurity potential in the same layer, and we assume that the scalar potential is short-ranged so that $u_I(\mathbf{Q})$ is actually independent of wave vector. The electron-impurity scattering time can be defined using the Born approximation for the self-energy¹⁷ where $\Sigma(\mathbf{k}, \omega) = -i\hbar/2\tau_{\mathbf{k}}$. In the presence of finite disorder, the scattering rate at the Fermi energy is used to define the small parameter of our perturbation

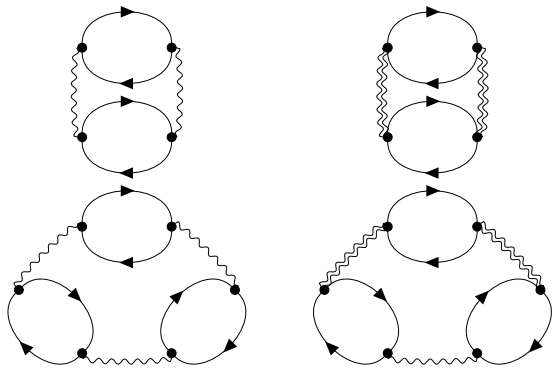


FIG. 2: Feynman diagrams for the correlation-energy of a bilayer-system whose quasiparticles interact via intralayer Coulomb interactions (single wavy lines) and interlayer Coulomb interactions (double wavy lines). Only the four lowest-order diagrams are shown here. Solid lines with arrows represent non-interacting Greens functions for quasiparticles.

theory, $1/(\tau\varepsilon_F) \ll 1$, where we here (and will continue to) drop the subscript on τ .

Our method for evaluating the force between two atomically-thin crystals consists of first calculating the ground-state energy as a function of interlayer separation distance, d , and then calculating the force by taking the first derivative

$$\mathcal{F} = -\frac{1}{2} \frac{\partial E}{\partial d}. \quad (6)$$

We can evaluate the ground-state energy by taking the zero temperature limit of the thermodynamic free-energy, Ω . The latter has a well-known perturbative formulation in the linked-cluster expansion¹⁷,

$$\Omega - \Omega_0 = -\frac{1}{\beta} \sum_{\ell > 0} \frac{1}{\ell!} \left(\frac{-1}{\hbar} \right)^\ell \int_0^{\hbar\beta} d\tau_1 \dots \int_0^{\hbar\beta} d\tau_\ell \quad (7)$$

$$\times \text{tr} \left\{ \rho_0 T_\tau \left[\hat{V}(\tau_1) \dots \hat{V}(\tau_\ell) \right] \right\}_0,$$

where ρ_0 is the non-interacting density-matrix, T_τ is the (imaginary) time-ordering operator, and $\hat{V}(\tau) = \mathcal{H}_{e\text{-imp}}(\tau) + \mathcal{H}_{e\text{-e}}(\tau)$ is the sum of the two interactions in our model within the interaction-picture of time evolution¹⁷. By applying Wick's theorem, we can express all contributions at order ℓ in terms of integrals over non-interacting Green's functions, the Coulomb interaction V , and the electron-impurity interaction u . We will make use of Feynman diagram techniques to efficiently calculate these contributions. We now have all the tools necessary to evaluate the interlayer force to any order in perturbation theory.

Before we consider the effects of weak-disorder on the interlayer forces, we reproduce the physics described by the Lifshitz' theory by examining the force between

two two-dimensional electron gases (2DEGs) within the random-phase approximation (RPA)¹⁸⁻²¹ and taking the limit of large interlayer distance, d . We thus ignore disorder and take $\hat{V}(\tau) = \mathcal{H}_{e\text{-e}}(\tau)$ within Eq. (7). The RPA can be understood as an expansion of the ground-state energy in powers of the small parameter r_s , and therefore gives a criterion for selecting which subset of Feynman diagrams at each order in m within Eq. (7) must be included in an approximation to a given order in r_s . The four lowest-order diagrams which contribute to the correlation energy are shown in Fig. (2). The full RPA approximation consists of summing all diagrams of this type, which at each order in ℓ contain ℓ bubble sub-diagrams. The degeneracy of the diagrams in Fig. (2) is such that the infinite series of these type of diagrams can be resummed into a logarithm of a simple function of the single bubble diagram. After taking the derivative of the RPA approximation for the correlation energy, we obtain the following integral expression for the force per layer between a bilayer-system containing a finite density of electrons and holes in each layer

$$\mathcal{F} = -\frac{\hbar L^2}{4\pi^2} \int_0^\infty dq d\omega \frac{q^2 V_{12}^2 \chi_0^2}{(1 - V_{11}\chi_0)(1 - V_{22}\chi_0) - V_{12}^2 \chi_0^2}. \quad (8)$$

Here, χ_0 is represented by the bubble sub-diagrams found in the four diagrams in Fig. (2) and describes the non-interacting density-density response function of each layer. The zero-temperature limit of χ_0 can be evaluated for parabolic-band effective mass models, and in the presence of both valence- and conduction-bands, $\chi_0 = \sum_\alpha \chi_0^\alpha$, where χ_0^α is the Lindhard-function²² of the α -particle species. The integral over frequency in Eq. (8) is over the imaginary frequency axis, and the arguments of $\chi_0^\alpha(q, i\omega)$ have been omitted for brevity. The application of Eq. (8) assumes that thermal equilibrium has been reached among the electrons and holes, which is usually several orders of magnitude faster than the electron-hole recombination time, and does not limit experimental observations. For arbitrary electron/hole densities and interlayer separation distance, Eq. (8) must be evaluated numerically. In Fig. (3) we present the results of numerical calculations for the pressure (*i.e.* force per area) between two layers of atomically-thin crystals with optically-induced densities of electrons and holes defined by r_s . We immediately notice that the force between layers is attractive and that the magnitude varies dramatically with interlayer separation distance. This is a particular feature of the type of dispersion force that derives from the instantaneous Coulomb interaction (typically called Van der Waals forces) instead of forces originating from the transverse and retarded part of the electromagnetic field (typically called Casimir forces). While Casimir forces act at larger distances than Van der Waals forces, they are significantly weaker and they are independent of the amount of impurities in the materials, and therefore are not addressed in this article.

To demonstrate that our RPA theory captures much of the physics contained within the Lifshitz theory, we now

evaluate Eq. (8) in the limit of large interlayer separation. Specifically, we will find the leading-order contribution to the interlayer force in the small parameter $1/(k_F d)$, where $k_F = \sqrt{k_F^e k_F^h}$ is the Fermi wave vector of the electron- and hole-Fermi-seas which are present in each layer after optical excitation and thermalization. The presence of e^{-2qd} in the numerator of Eq. (8) restricts the important range of q in the integral to $q \lesssim 1/d$, which bears the physical interpretation that 2D in-plane charge perturbation waves at wavelengths which are short compared to the interlayer distance appear averaged out on the adjacent plate and thus will not contribute to forces. Long wavelengths, however, will not appear as averaged out and will therefore contribute to interlayer forces. In the limit $k_F d \gg 1$, the dominant contribution to interlayer forces will then come from long in-plane wavelengths and this thus restricts the relevant part of phase space to small values of q . In this region of phase-space we are permitted to approximate χ_0^α by its *dynamic* long-wavelength limit (*i.e.* $\omega > q$, $q \rightarrow 0$) which gives the leading-order contribution to the force. In the dynamic long-wavelength limit the non-interacting density-density-response function of band α is given by

$$\chi_0^\alpha(q, i\omega) = -\frac{\rho_\alpha q^2}{m_\alpha \omega^2}, \quad (9)$$

where ρ_α is the two-dimensional density of charged quasiparticles in band α . It is then straightforward to evaluate Eq. (8) analytically to obtain the leading-order in $1/(k_F d)$

$$\mathcal{F} = -\frac{\hbar e \xi_1 L^2}{8\sqrt{2}\pi m} \left(\frac{\sqrt{\rho}}{d^{7/2}} \right) \quad (10)$$

where $\xi_1 \approx 0.315$, ρ is the total two-dimensional quasiparticle density in each layer, and we have taken $m_h = m_e = m$ for simplicity. We can introduce the three-dimensional density, $\rho_{3D} = \rho/d$, in Eq. (10) to compare with Lifshitz' theory and we immediately see that we have correctly reproduced the power-law for the interlayer force in terms of interlayer separation and quasiparticle density (*i.e.* $\mathcal{F} \propto \sqrt{\rho_{3D} d^{-3}}$). In future sections we will describe how these power laws are altered by the presence of impurities. Despite the obvious utility of simple formulas like Eq. (10), the derivation demonstrates that only the long-wavelength excitations (*i.e.* plasmons) are accounted for, while finite q excitations (*e.g.* non-coherent particle-hole excitations) are neglected. Indeed, Eq. (10) is only reasonable in the limit $1/(k_F d) \ll 1$, and outside of this regime the interlayer forces are more accurately described by numerically evaluating Eq. (8).

III. IMPACT OF DISORDER ON VDW FORCES: THE 'DIFFUSION'

In this section we lay out the basic elements of a many-body theory for the impact of weak-disorder on

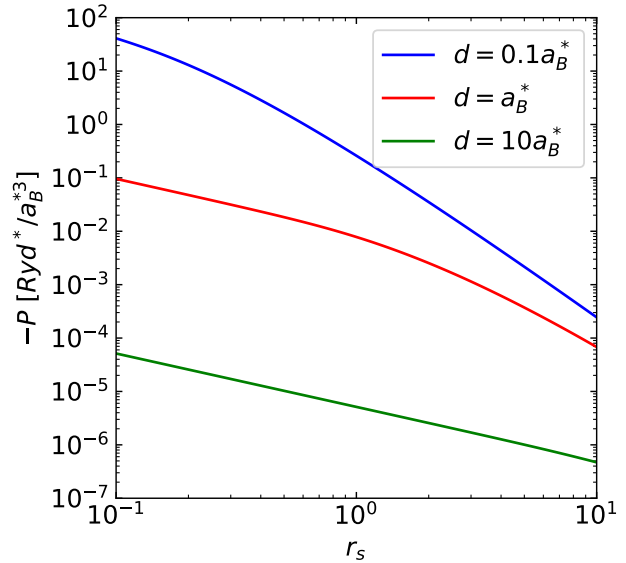


FIG. 3: A plot of interlayer forces *vs.* the density of optically-induced quasiparticles in a disorder-free bilayer-system. On the vertical axis is the force per area in units of effective Rydbergs per effective Bohr radius cubed. On the horizontal axis is the dimensionless parameter r_s which is inversely proportional to the density of optically induced quasiparticles. Explicit definitions for r_s , Ryd^* , and a_B^* can be found in the main text.

the interlayer Van der Waals forces between atomically thin crystals. Specifically, we begin by introducing the small parameter (*i.e.* $1/\varepsilon_F \tau$) of the electron-impurity and hole-impurity interaction within the context of the first-order Born approximation for the self-energy. We then identify the most relevant Feynman diagrams which contribute to interlayer dispersion forces within the regime of $r_s < 1/\varepsilon_F \tau$. These diagrams contain an infinite series of ladder diagrams, and we discuss the solution of the Bethe-Salpeter equation for the vertex correction of the density-response function in the limit of short-range impurity potentials. Surprisingly, we find that disorder tends to *weaken* the magnitude of Van der Waals forces, in contrast to the effect of disorder on other phenomena which arise due to interlayer interactions (*e.g.* Coulomb drag).

The electron-impurity and hole-impurity scattering-rate can be defined by the first-order Born approximation (1BA) for the self-energy. In this approximation the self-energy is purely imaginary, $\Sigma(\mathbf{k}, \omega) = -i\hbar/2\tau_{\mathbf{k}}$. For simplicity, we will take the hole's and electron's impurity scattering rates to be equal, although this condition is easily relaxed if required. The 1BA is given by the Feynman diagrams depicted in panel a) and b) of Fig. (5). Explicitly, the 1BA for the scattering rate at the Fermi

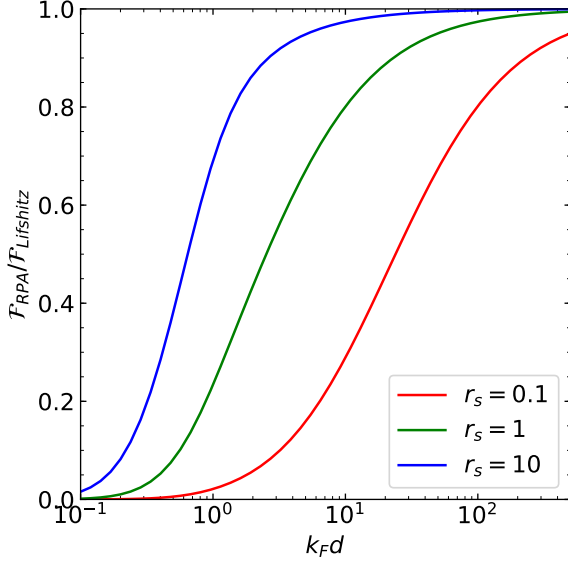


FIG. 4: Ratio of the interlayer force in the random-phase approximation (RPA), \mathcal{F}_{RPA} , calculated numerically using Eq. (8), divided by the interlayer force in the leading-order-in- $(k_F d)^{-1}$ approximation, $\mathcal{F}_{Lifshitz}$. The former is given by Eq. (8) and the latter by Eq. (10). The more accurate RPA approximation predicts much smaller interlayer attraction unless $k_F d \gg 1$, in which case both approximations give the same result.

energy is

$$\frac{1}{\tau} = \frac{\nu_\alpha}{2\hbar\pi} \rho^{imp} |u|^2 \quad (11)$$

where ν_α is the two-dimensional density-of-states at the Fermi-surface of a single spin- and valley-resolved band, and $\rho^{imp} = \lim_{Q \rightarrow 0} [\rho_I(\mathbf{Q})]$. In obtaining Eq. (11) we have made two assumptions. First is that the impurity potential is short-ranged, such that the Fourier transform of the potential which appears in Eq. (5), $u_I(\mathbf{Q})$, becomes independent of wave vector. Second is that the impurity potential at any two different points is uncorrelated, such that the average over the probability distribution governing the impurity potential leads to $\langle \rho_I(\mathbf{Q}) \rho_I(-\mathbf{Q}) \rangle_{imp} = N_{imp}$, where N_{imp} is the number of impurities in layer I . These are standard approximations for treating quenched disorder in solids¹⁷.

We next consider how to incorporate quasiparticle-quasiparticle interaction diagrams and quasiparticle-impurity interaction diagrams into an approximation for the dispersion force between atomically thin crystals. In the last section we identified the leading-order-in- r_s contribution to interlayer forces as the derivative of the RPA diagrams for the ground-state energy. In order to work with a well controlled perturbation theory we will restrict our selection of diagrams to the case when $r_s \ll 1/(\tau\varepsilon_F)$. This allows us to obtain a well controlled theory in both small parameters. The key is to not alter the order in

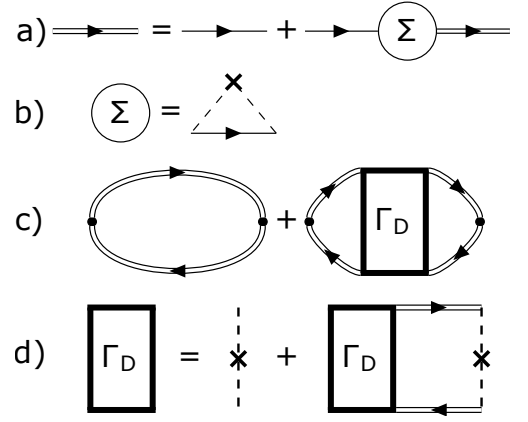


FIG. 5: Feynman diagrams for the leading-order in $1/\varepsilon_F \tau$ corrections to interlayer dispersion forces from impurity-quasiparticle interactions. Panel a) shows the diagrams for the Dyson equation for the self-energy. Single lines with arrows are non-interacting Greens functions and double lines with arrows are the non-interacting Greens functions dressed by scattering with impurities. Panel b) shows the proper self-energy in the first Born approximation. Each dashed line with a single cross represents the (disorder averaged) scattering off of the impurity potential. Panel c) shows the diagrams which contribute to the non-interacting density-response function in the leading-order in $1/\varepsilon_F \tau$. Panel d) shows the diagrammatic representation of the Bethe-Salpeter equation for the *diffusion* contribution, *i.e.* the ladder-diagram vertex-correction $\Gamma_D(q, \omega)$

r_s of a diagram by adding any particular quasiparticle-impurity interaction line. We can accomplish this feat by adding to the RPA diagrams a nearly identical set of diagrams in which the non-interacting density-density-response function is *dressed* by quasiparticle-impurity interaction lines between the electron propagator and hole propagator which form each bubble. As long as these *vertex-correction* quasiparticle-impurity lines do not cross each other, they can be summed to infinite order and together they give the leading-order in $1/(\tau\varepsilon_F)$. The sum of all ladder Feynman diagrams for the density-density response function of each layer I is represented in Fig. 5c) and 5d). The latter is the diagrammatic representation of the Bethe-Salpeter equation

$$\Gamma_{\mathbf{k}, \mathbf{k}'}^D(q, \omega) = \Gamma_{\mathbf{k}, \mathbf{k}'}^0 + \sum_{\mathbf{k}''} \Gamma_{\mathbf{k}, \mathbf{k}''}^0 \Pi_{\mathbf{k}''}(q, \omega) \Gamma_{\mathbf{k}'', \mathbf{k}'}^D(q, \omega) \quad (12)$$

where

$$\Pi_{\mathbf{k}''}(q, \omega) = \frac{1}{\hbar^2 L^2} G^R(\mathbf{k}'' + \mathbf{q}, \varepsilon_F + \omega) G^A(\mathbf{k}'', \varepsilon_F) \quad (13)$$

and where $G^{R/A}(\mathbf{k}, \omega) = [\omega - \hbar^{-1} \xi_{\mathbf{k}\alpha} \pm i/2\tau]^{-1}$ and $\xi_{\mathbf{k}\alpha} = \varepsilon_{\mathbf{k}\alpha} - \varepsilon_F$. The Bethe-Salpeter must usually be solved self-consistently for an arbitrary impurity potential, but in this case can be solved as a result of the bare-scattering-amplitude being independent of momentum

$\Gamma_{\mathbf{k},\mathbf{k}'}^0 = \rho^{imp}|u_I|^2$. In the regime where disorder gives significant contributions to the density-response of a system, $\omega < 1/\tau$ and $q < 1/v_F\tau$, straight-forward calculations²³ yield $\Gamma^D(q, \omega) = \Gamma^0(q) / [-i\omega\tau + \tau Dq^2]$ where the diffusion constant is defined in 2D as $D = v_F^2\tau/2$. The diffusion pole present in $\Gamma^D(q, \omega)$ at $\omega = -iDq^2$ is also present in the disordered density-response function of layer I that is obtained by summing the diagrams in Fig. 5c) and yields

$$\chi_D(q, \omega) = -\nu_0 \frac{Dq^2}{-i\omega + Dq^2} \quad (14)$$

where ν_0 is the total density-of-states at the Fermi energy in layer I .

We can now evaluate the effect of weak-disorder on the dispersion force between two atomically-thin crystals by numerically evaluating Eq. (8) after replacing $\chi_0(q, i\omega)$ by $\chi_D(q, i\omega)$ in the region of phase-space $\omega < 1/\tau$ and $q < 1/v_F\tau$. In Fig. (6) we plot the ratio of the interlayer force in the presence of disorder, \mathcal{F}_{dirty} , to the force in the absence of disorder, \mathcal{F}_{clean} . We find that the interlayer attraction is reduced in magnitude by the presence of quasiparticle-impurity interactions, which we will analyze in more detail below. We also find that $\mathcal{F}_{dirty}/\mathcal{F}_{clean}$ is reduced as d increases. This occurs because the presence of e^{-2qd} in Eq. (8) which originates from the form of the 2D in-plane Fourier transform of the interlayer Coulomb interaction. This factor restricts the density-fluctuations which contribute to interlayer forces to wave vectors $q \lesssim 1/2d$, and as d is increased more of this region of phase-space lies in the region governed by the disordered density-density response, $q < 1/v_F\tau$. We will now show that this phase-space effect is also responsible for a change in the power-laws for the dispersion forces at large interlayer separation distances; in the presence of disorder, the 'Lifshitz' limit for forces between 2D planes presented in Eq. (10), $\mathcal{F} \propto d^{-7/2}$, is altered.

Perhaps the most surprising aspect of the numerical results presented in Fig. (6) is that disorder *decreases* the magnitude of interlayer forces. This is in contrast to the effect of disorder on other phenomena, like Coulomb drag, which also originates from interlayer quasiparticle-quasiparticle interactions. In the case of Coulomb drag, the conventional cartoon-picture of the effect of disorder is that the change in the density-response function from the non-interacting limit $\chi_0(q, i\omega)$ to the disordered limit $\chi_D(q, i\omega)$ represents a change from ballistic to diffusive motion of the quasiparticles. Indeed, the disordered density-density-response function can be derived from semiclassical arguments using the diffusion equation¹⁵. Since quasiparticles in neighboring layers which experience diffusive motion tend to spend longer periods of time near to each other, they interact more strongly and this increases the Coulomb drag (*i.e.* disorder tends to enhance the transresistivity). However, since the interlayer forces are decreased in magnitude by the presence of disorder, we find that the cartoon-picture of the effect of disorder cannot be imported to understand our

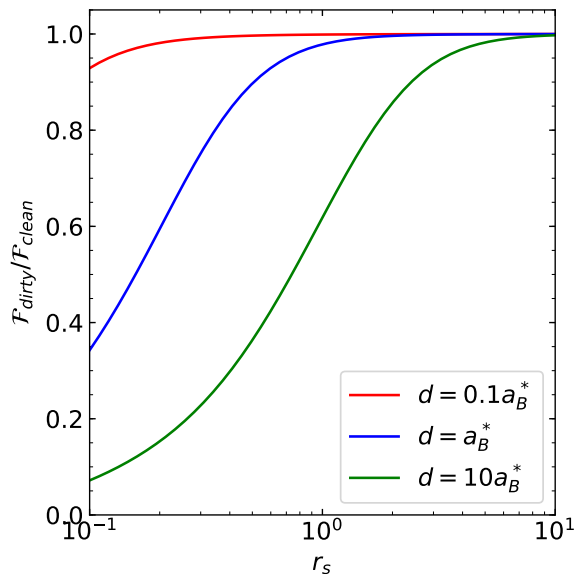


FIG. 6: Ratio of the interlayer force in the presence of disorder, \mathcal{F}_{dirty} , to the interlayer force with no disorder, \mathcal{F}_{clean} , plotted against the interaction parameter r_s which is inversely proportional to the optically-induced quasiparticle density in each layer of a bilayer. The three curves are for three different values of the interlayer separation distance, d , in units of the effective Bohr radius a_B^* . The values of both \mathcal{F}_{dirty} and \mathcal{F}_{clean} are calculated numerically using Eq. (8). In the former, the density-response is given by the disordered limit, $\chi_D(q, \omega)$, for $\omega < 1/\tau$ and $q < 1/v_F\tau$.

case of interest. The reason why disorder decreases interlayer forces while increasing the interlayer Coulomb drag, is most simply identified by again examining the large d limit of the two quantities. Specifically, while both Coulomb drag and the interlayer force depend on the density-response function, the leading order in $1/(k_F d)$ contribution to Coulomb drag come from the *static* limit ($\omega < q$, $q \rightarrow 0$) of $\chi(q, i\omega)$ while the analogous contribution to the interlayer force comes from the *dynamic* limit ($\omega > q$, $q \rightarrow 0$) of $\chi(q, i\omega)$. By following similar steps as we took to derive the disorder-free expression presented in Eq. (10), we find the following leading-order expression

$$\mathcal{F}_{dirty} = -\frac{\hbar e^2 \xi_2 L^2 \tau}{4\pi m} \left(\frac{\rho}{d^4} \right) \quad (15)$$

where $\xi_2 \approx 0.768$ and ρ is the total two-dimensional density of quasiparticles in each layer and we have again taken $m_e = m_h = m$ for simplicity. Notice that the interlayer force now decays more quickly with distance than in the absence of disorder. This qualitative change is a direct result of the transition of electron/hole motion from ballistic to diffusive.

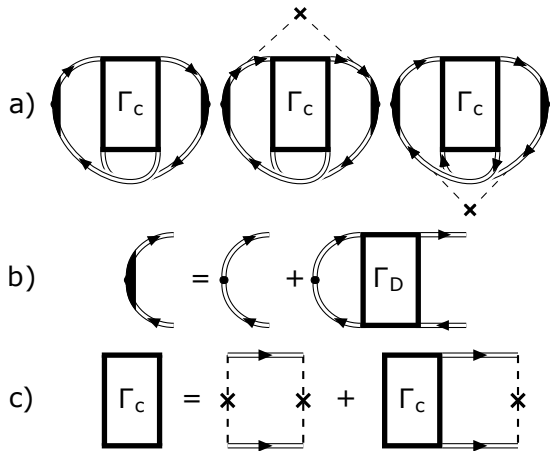


FIG. 7: Feynman diagrams representing the *cooperon* contributions to the non-interacting density-response function from scattering of electron/holes off of the impurity potential. Panel a) shows the three diagrams that contribute at subleading order in $1/\epsilon_F\tau$. Panel b) shows the diagrams describing the *diffuson* dressing of the density-fluctuation operator. Panel c) shows the Bethe-Salpeter representation of the maximally-crossed diagrams that represent the vertex-correction, $\Gamma_C(q, \omega)$.

IV. QUANTUM INTERFERENCE EFFECTS ON VDW FORCES: THE 'COOPERON'

In the previous section we developed a theory for interlayer dispersion forces between the layers of a bilayer-system of atomically-thin crystals which have uncorrelated and short-ranged disorder. We summed an infinite set of Feynman diagrams by solving the Bethe-Salpeter equation and thus obtained the *diffuson* vertex-correction of the density-density-response function to leading-order in $1/(\epsilon_F\tau)$. In this section we will sum the class of diagrams which corresponds to the subleading-order terms for the interlayer dispersion force in powers of $1/\epsilon_F\tau$. These diagrams are familiar from the theory of weak-localization and together they constitute the *cooperon* vertex-correction. Despite being of lower order in the small-parameter governing the impurity-quasiparticle interaction, they are known to be responsible for a logarithmic divergence in the longitudinal resistivity of two-dimensional conductors¹², which motivates us to consider them here as well. The cooperon contributions to the density-density-response function are obtained by summing the 'maximally crossed' vertex-correction; this infinite set of diagrams is illustrated in Fig. 7c). These diagrams represent the quantum interference of a wavepacket of charge-density which interferes with itself while traversing along the time-reversed path. This requires the system to have a time-reversal symmetry present in order for phase coherence to be maintained in-between collisions of the wavepacket with different impurities. As previously mentioned, these diagrams give

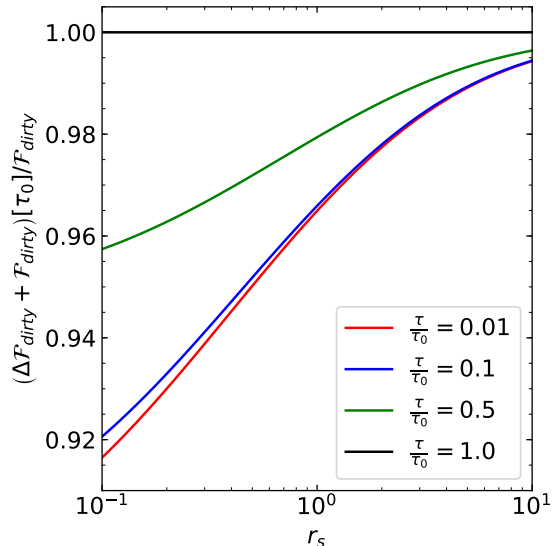


FIG. 8: The fractional change in the interlayer-dispersion force when the maximally crossed (*i.e.* weak-localization) diagrams are included. Notably, the logarithmic divergence which appears in the longitudinal resistivity of two-dimensional conductors is not present here. Instead, the *cooperon* diagrams have a similar, but weaker, effect as the *diffuson* diagrams, where both tend to reduce the magnitude of interlayer attractive forces.

a logarithmic divergence in the resistivity (which is proportional to the current-density response-function), and indeed a similar phenomena happens in our case of interest. Specifically, the subleading-order contribution to the density-density-response function yields a logarithmic divergence in the Diffusion constant. When both the diffuson and cooperon contributions to the density-density-response function are included²⁴, the functional form of $\chi_D(q, \omega)$ remains the same as presented in the last section except that D gets an additional contribution which depends on frequency:

$$\delta D(\omega) = \frac{-1}{4\pi^2\hbar\nu_0} \log \left[\frac{1 + 2\tau\omega}{(\tau/\tau_0)^2 + 2\tau\omega} \right] \quad (16)$$

where ν_0 is the total two-dimensional density-of-states of all quasiparticles in layer I . Just as in the case of the cooperon contribution to the longitudinal resistivity, the logarithmic divergence we obtain is cutoff by the inelastic scattering time of the quasiparticles, τ_0 . This time-scale is determined, for example, by the quasiparticle-quasiparticle scattering rate, and is responsible for destroying the phase-coherence of the propagating (and time-reversed propagating) wavepacket on very long time-scales, $\tau_0 > \tau$. This form of the disordered response-function is only a reasonable approximation in the range where $\omega < 1/\tau$ and $q < 1/v_F\tau$.

We numerically calculate the interlayer dispersion

forces using the disordered density-density-response function including the renormalized diffusion constant, $D \rightarrow D + \delta D(\omega)$ and display the results in Fig. (8). This demonstrates that the maximally-crossed diagrams tend to further reduce the magnitude of interlayer forces. More surprisingly, perhaps, there is no logarithmic divergence in the interlayer force, in contrast to what happens when using the analogous approximation for the longitudinal conductivity. This is surprising in light of the well-know relationship, $\sigma_{dc} = \lim_{q \rightarrow 0} (q^2/\omega^2) \chi_D(q, \omega)$, which follows from the presence of global gauge-symmetry. However, while the conductivity is the response of the system to an external electric field whose frequency we can always fix to zero, in contrast the interlayer dispersion force is an *integral over all frequency* of density-fluctuations in both layers (it is the Coulomb interaction between these density-fluctuations which yield the dispersion force). And when the logarithmic divergence in $\chi_D(q, \omega)$ is integrated over frequency, the result is simply a finite and $\lesssim 10$ percent reduction in the interlayer force's magnitude.

V. SUMMARY AND DISCUSSION

We developed a many-body theory for the dispersion forces between atomically-thin crystals with weak disorder. Such systems can be realized within Van der Waals crystals²⁵ (*e.g.* graphene, transition-metal dichalcogenides, etc.) which form multilayer-systems with very weak interlayer hybridization; a property which has allowed for optically induced interlayer strain, originating from dispersion forces, to be observed recently⁶. In these systems *dispersion* forces arise due to Coulomb interactions between fluctuations in the charge-density of neighboring layers. The linked-cluster expansion method was used to approximate the correlation energy of a bilayer-system and the force between the layers of the bilayer-system was obtained by taking a derivative of the correlation energy with respect to interlayer separation distance. Within this method, contact with existing theory was made by considering the limit of large interlayer separation or high quasiparticle density, wherein scaling laws consistent with those found by Lifshitz for two thick slabs separated by a distance d were found² in the absence of disorder.

In the high-density limit, the random-phase approximation bubble diagrams give the leading-order contribution to the disorder-free interlayer dispersion force. To account for disorder, we have summed an infinite series

of ladder diagrams by solving the Bethe-Salpeter equation. These ladder diagrams form the *diffuson* contribution to the vertex-correction of the density-density response function (*i.e.* the bubble), and yield the leading-order-in- $1/(\varepsilon_F \tau)$ theory. Numerical evaluation of the interlayer dispersion force shows that, surprisingly, interlayer forces are *weakened* by disorder. This is in contrast to the more conventional case²⁶ in which Coulomb interactions become more important when electron motion becomes diffusive rather than ballistic. We explain this behavior by considering the analytic structure of the density-response function in the small frequency and wavevector limit. We find that the diffusive motion of electrons and holes leads to a qualitative change in the scaling laws for the interlayer dispersion force as a function of quasiparticle density and interlayer separation distance. Subsequently, the impact of the higher-order vertex-correction diagrams was investigated. Specifically, maximally-crossed diagrams which are known to produce logarithmic divergences in the longitudinal resistivity of two-dimensional metals (*i.e.* weak localization diagrams) are found to be much less important for interlayer dispersion forces.

Optical control of electron and hole populations yields a convenient control knob for manipulating the interlayer separation distance of Van der Waals crystals. In future calculations we will investigate the possibility of inducing interlayer dispersion forces by doping heterostructures with electrostatic gates. While these systems include interlayer electrostatic forces which compete with dispersion forces, the latter are not reliant on equal populations of electrons and holes and can hopefully still be observed. Through electrostatic gating the role of the excitonic spectrum in the formation of strains could be differentiated from the optically-induced strains presented in this publication. In order to complement this investigation of the role of excitons, it would furthermore be interesting to investigate the qualitative changes in interlayer dispersion forces which are present in multilayer systems with more exotic ground state wavefunctions, such as are present in bilayer exciton condensates.

Acknowledgments

J.v.M. acknowledges support by the Deutsche Forschungsgemeinschaft (DFG, German Research Foundation) under Germany's Excellence Strategy – EXC-2111–390814868. J.R.T. acknowledges financial support from the Swiss National Science Foundation.

* Electronic address: jtolsma@phys.ethz.ch

¹ R. Eischenschitz and F. London, *Zeitschrift für Physik* **60**, 491 (1930).

² E. M. Lifshitz, *Sov. Phys. JETP* **2**, 73 (1956).

³ J. D. Jackson, *Classical Electrodynamics* (John Wiley & Sons Inc, 1998), ISBN 047130932X.

⁴ M. Kozina, T. Hu, J. S. Wittenberg, E. Szilagy, M. Trigo, T. A. Miller, C. Uher, A. Damodaran, L. Martin,

- A. Mehta, et al., *Structural Dynamics* **1**, 034301 (2014).
- ⁵ I.-C. Tung, A. Krishnamoorthy, S. Sadasivam, H. Zhou, Q. Zhang, K. L. Seyler, G. Clark, E. M. Mannebach, C. Nyby, F. Ernst, et al., *Nature Photonics* (2019).
- ⁶ E. M. Mannebach, C. Nyby, F. Ernst, Y. Zhou, J. Tolsma, Y. Li, M.-J. Sher, I.-C. Tung, H. Zhou, Q. Zhang, et al., *Nano Letters* **17**, 7761 (2017).
- ⁷ B. Narozhny and A. Levchenko, *Reviews of Modern Physics* **88** (2016).
- ⁸ J. P. Eisenstein and A. H. MacDonald, *Nature* **432**, 691 (2004).
- ⁹ M. Kellogg, I. B. Spielman, J. P. Eisenstein, L. N. Pfeiffer, and K. W. West, *Physical Review Letters* **88** (2002).
- ¹⁰ D. Laroche, G. Gervais, M. P. Lilly, and J. L. Reno, *Science* **343**, 631 (2014).
- ¹¹ J. Klimeš, D. R. Bowler, and A. Michaelides, *Physical Review B* **83** (2011).
- ¹² L. P. Gor'kov, A. I. Larkin, and D. E. Khmel'nitskii, *JETP lett.* **30**, 228 (1979).
- ¹³ B. Altshuler and A. Aronov, *Zh. Eksp. Teor. Fiz* **77**, 2028 (1979).
- ¹⁴ B. Altshuler and A. Aronov, *Solid State Communications* **30**, 115 (1979).
- ¹⁵ G. Giuliani and G. Vignale, *Quantum Theory of the Electron Liquid* (Cambridge University Press, 2005).
- ¹⁶ T. B. Arp, D. Pleskot, V. Aji, and N. M. Gabor, *Nature Photonics* (2019).
- ¹⁷ G. D. Mahan, *Many-Particle Physics* (SPRINGER NATURE, 1990), ISBN 0306434237.
- ¹⁸ D. Bohm and D. Pines, *Physical Review* **82**, 625 (1951).
- ¹⁹ D. Pines and D. Bohm, *Physical Review* **85**, 338 (1952).
- ²⁰ D. Bohm and D. Pines, *Physical Review* **92**, 609 (1953).
- ²¹ D. Pines, *Physical Review* **92**, 626 (1953).
- ²² J. Lindhard, *Dan. Vid. Selsk Mat.-Fys. Medd.* **28**, 8 (1954).
- ²³ E. Akkermans and G. Montambaux, *Mesoscopic Physics of Electrons and Photons* (Cambridge University Press, 2007).
- ²⁴ C. D. Castro and R. Raimondi, *Statistical Mechanics and Applications in Condensed Matter* (Cambridge University Press, 2015).
- ²⁵ A. K. Geim and I. V. Grigorieva, *Nature* **499**, 419 (2013).
- ²⁶ P. A. Lee and T. V. Ramakrishnan, *Reviews of Modern Physics* **57**, 287 (1985).